Available online at www.sciencedirect.com



Manufacturing Letters

Manufacturing Letters 41 (2024) 810-821



52nd SME North American Manufacturing Research Conference (NAMRC 52, 2024)

Predictive Models for 3D inkjet Material Printer using Automated Image Analysis and Machine Learning Algorithms

Mutha Nandipati^{a,b}, Michael Ogunsanya^{a,b}, Salil Desai^{a,b,*}

^aDepartment of Industrial and Systems Engineering, North Carolina Agricultural and Technical State University, Greensboro, NC 27411, USA ^bCenter of Excellence in Product Design and Advanced Manufacturing, North Carolina Agricultural and Technical State University, Greensboro, NC 27411, USA

* Corresponding author. Tel.: +1-336-285-3725; fax: +1-336-334-7729. E-mail address: sdesai@ncat.edu

Abstract

Additive manufacturing (AM) is a smart manufacturing process to fabricate components with high precision, minimal post-processing, and increased component complexity in a variety of materials. This research focuses on developing automated image analysis and predictive models for a widely used 3D material inkjet printing (IJP) process. The interplay of four input process parameters, which include frequency, voltage, temperature, and meniscus vacuum, on the output metrics of the inkjet printer was evaluated using statistical measures (ANOVA). Droplet types were classified as no drop, satellite drop, and normal drop using four machine learning classifiers, including random forest, support vector classifier, k-nearest neighbor, and decision trees. Hyperparameter tuning was performed for each model for over 486 data points. Regression predictive models were developed for both ink droplet velocity and volume with three linear models (linear, lasso, and ridge regression) and four non-linear models (random forest, decision tree, support vector regression, and k-nearest neighbor). Mean squared error and the coefficient of determination, r-squared value, were used to evaluate the performance of the predictive models. For the drop type classification models, k-fold of 5 yielded the highest accuracy for the RF, KNN, and DT models of around 98%. Similarly, for the regression based predictive models RF, DT and KNN accuracy results ranged from 97 to 99%. All the machine learning models were validated with experimental data with high prediction accuracies accuracy. This research serves as a foundation for developing design guidelines for 3D material inkjet printing with applications in biosensors, flexible electronics, and regenerative tissue engineering.

© 2024 The Authors. Published by ELSEVIER Ltd. This is an open access article under the CC BY-NC-ND license (https://creativecommons.org/licenses/by-nc-nd/4.0)

Peer-review under responsibility of the scientific committee of the NAMRI/SME.

Keywords: additive manufacturing; hyperparameter optimization; inkjet 3D printing; machine learning; predictive models.

1. Introduction

3D printing, also known as additive manufacturing (AM), builds three-dimensional solid objects, layer-by-layer, using different materials such as polymers, composites, ceramics, and metals. There are different types of additive manufacturing processes, which include photo-polymerization processes, extrusion-based systems, powder bed fusion processes, material

jetting processes, binder jetting processes, sheet lamination processes, and direct write technologies [1]–[3]. Inkjet 3D printing (IJP) is one of the most popular AM techniques that deposits micrometre-scaled material-laden droplets with very high precision [4]–[11]. Of all the AM processes, inkjet printing has emerged at the frontline due to its unique features of low cost, high pattern precision and resolution, scalability,

compatibility with different substrates, reduced postprocessing, and non-contact approach.

Nomenclature

v voltage in volts

f jetting frequency in kHz

t cartridge ink temperature in degree Celsius

mv meniscus vacuum in inches H_2O V velocity of the ink droplet in m/s Vol. volume of the ink droplet in μ m³

LR linear regression RF random forest

SVM support vector machine SVR support vector regressor

DT decision tree KNN k-nearest neighbor

The 4th industrial revolution, or Industry 4.0, encompasses a variety of technologies to transform the manufacturing industry [12]. It involves concepts such as inter-machine communication, the internet of things to enable automation, and developing machines with the minimum technical intervention of humans [13], [14]. Extending this concept to the additive manufacturing process, physics-based models have been developed for IJP to produce micro and nanoscale dimensions [11], [15]–[17].

There are two different mechanisms by which inkjet printers generate droplets, which include Continuous Inkjet (CIJ) and Drop-on-Demand Inkjet (DoD) printing [13]. In a CIJ system, a stream of droplets is ejected continuously under an applied electric field and a charging electrode. In a DoD printing system, the droplet can be ejected based on print demand by a voltage waveform [14]. In the IJP process, the liquid material is jetted out from the printer head (carrying an ink-filled cartridge) in a sequence of micro-droplets via a micrometersized nozzle head, which are then solidified on the substrate. The deposited materials are in the form of chemical solutions and colloidal dispersions. The major actuation mechanisms of the inkjet nozzle head include thermal, piezoelectric, and electrohydrodynamic. The benefits of IJP are compatibility with elastomers, maskless processing, reduced manufacturing costs, and the fabrication steps [18]. In a continuous inkjet (CIJ) printer, a high-pressure pump pushes ink from a nozzle, creating continuous ink droplets. The droplets are surrounded by an electrostatic field created by a charging electrode. Under the influence of the electrostatic deflection plates, the charged droplets can pass through the electrostatic field and are finally printed on the substrate [19], [20]. The unused droplets are pushed back to the ink chamber. CIJ is an aged technology and normally used for commercial products and packages. The drop-on-demand (DoD) printers are either thermal or piezoelectric in type. In thermal DoD printers, a pulse current can rapidly vaporize the ink to form a bubble, producing a high pressure to propel a droplet of ink printed on the substrate [21]. On the other hand, piezoelectric printers use piezoelectric heads with an ink chamber behind each nozzle. A voltage is applied, which generates a pressure pulse, ejecting ink droplets from the nozzle [22]. The advantage of the piezoelectric inkjet is its wider variety of inks compared to the thermal inkjet, as there is no need for volatile components in the inks [23]. In this

research, we focus on DoD inkjet printers as they are primarily used in 3D printing of functional parts. The print quality in DoD inkjet AM process largely depends on several factors, of which piezoelectric voltage (referred to as voltage from here on), jetting frequency (referred to as frequency from here on), cartridge temperature (also referred to as ink temperature), and meniscus vacuum maintained at the nozzles are the most influential. These factors will influence the ink droplet's type, velocity, and volume. Depending on the process parameters, droplets may not eject from the nozzles (no-droplet condition), satellites may follow the regular drops, or they may come out like healthy normal droplets [24], [25]. The resolution of the printed object also depends on the drop's velocity and volume. Analysis of drop-on-demand piezo inkjet printers conducted by Kang et al., [26] found that increasing the piezoelectric voltage increased the ejection velocity with associated generation of satellite drops. Cooling the ink decreased the drop velocity while diminishing the satellite drops. The videos obtained from different combinations of voltage and frequency were processed using image analysis, and it was discovered that jetting behavior changed with reference to voltage and frequencies [15]. Optimal voltage and frequencies are required to eject normal droplets. A study of the jetting evolution of inkjet printers [27] shows that drop velocity increases with an increase in cartridge temperature. For the behavior of droplet impacting substrate, researchers have performed numerous research work studies [28], [29]. Du et al. [30] studied the kinetics of the droplets, and Xiao et al. [31] investigated the droplet collision kinetics. All these studies show the root cause of the print failure as either droplet type, droplet velocity, droplet volume, or a combination of some or all of these. The most challenging part of inkjet printing is achieving a consistent droplet deposition quality [32]. A machine learning approach was utilized by Caggiano et al. [33] to develop online fault prediction with automatic image processing in for timely identifying material defects. Their research was conducted by capturing images during the layer-by-layer SLM process. Wu and Xu [34] utilized predictive models for predicting droplet velocity and volume using ensemble learning. Lin et al. [35] evaluated the two aspects of droplet profiles: droplet shape and temperature, using radial basis function neural networks. Machine learning has been used in different fields to understand the complexity and nonlinearity that exist in a system when sufficient data are provided [36]-[38]. This research focuses on automated image analysis and building predictive models to improve the droplet quality of the DoD inkjet printing process. Furthermore, ML models are utilized to predict droplet characteristics, such as droplet velocity and volume, based on input parameters. Unlike most works found in the literature where one or at most two influencing inkjet parameters were considered, this work used four (4) most influential factors such as voltage, frequency, ink temperature, and meniscus vacuum to predict both qualitative (ink droplet type) and quantitative (volume and velocity) characteristics of the ink droplet. Moreover, a comprehensive treatment of machine algorithms was performed for predicting qualitative and quantitative measures for of droplet performance. Thus, this paper elucidates the translation of automated image analysis into seamless predictive models that

can be implemented in real-world industrial 3D printing settings.

2. System description

Experiments were conducted on the Fuji Dimatix DMP 2850 inkjet 3D printer as shown in Fig.1a. The Dimatix materials printer (DMP) can handle a wide variety of fluids, including aqueous-based, solvent-based, UV-curable fluids, biological solutions, and particle suspensions. Printing efficacy was optimally achieved by choosing fluid characteristics that include a viscosity range of 4-8 cps, surface tension range of 28-32 dynes/cm. The cartridge, as shown in Fig. 1b, can handle chemically compatible materials such as aliphatic hydrocarbons, aromatic hydrocarbons, aliphatic alcohols, ketones, ethers, acrylates, and glycols.

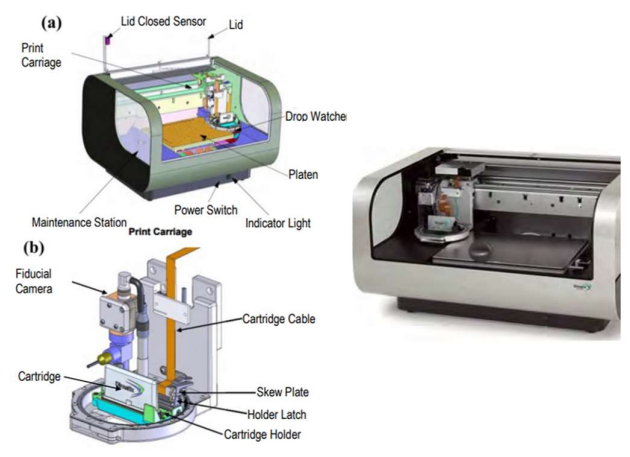


Fig. 1. (a) Dimatix 2850 printer, (b) ink cartridge. [39]

With piezoelectric drop-on-demand inkjet technology, a drop volume of 2.4 pL with a single dot size of 30 µm using 12 jets of nozzles can achieve 75 DPI resolution. The print head is equipped with a built-in heater and thermistor to heat the ink and measure the temperature. All these special features make this printer capable of manufacturing flexible electronic circuits, RFID antennas, 3D printed materials, and DNA arrays. Substrates up to 25mm thick with a printable area of 210 mm x 260 mm can be used to achieve a print repeatability of +/- 25 μm. To observe the drop and print qualities, two types of cameras are used: drop watcher and fiducial cameras, as shown in Fig. 2a and 2b. The drop-watcher camera allows direct viewing of the jetting nozzles and the actual jetting of the fluid. The fiducial camera aids in depositing a pattern on a prepatterned substrate, in jetting a layer with a different cartridge material or inspecting the printed features.





Fig. 2. (a) Drop watcher camera, (b) Fiducial camera.

3. Methodology

The research progressed through a series of activities, including setting up and conducting experiments. These involved the extraction of output parameters of drop characteristics (no drop, normal drop, and satellite drop), drop velocity, and drop volume, image acquisition and processing, and building droplet prediction machine learning models.

3.1. Design of experiment

Full factorial design was used to choose various combinations of voltage, frequency, ink temperature, and meniscus vacuum to study the output parameters, which include drop quality, velocity, and volume. A design matrix with four factors (voltage, frequency, ink temperature, and meniscus vacuum) at three levels (low, medium, and high) and six replications was used. A total of 486 experimental runs were conducted ($3^4 \times 6 = 486$). All four input parameters contributed equally among all 486 datasets. Experiments were conducted on the Fujifilm Dimatix DMP 2850 inkjet 3D printer. Videos were captured from the drop watcher camera (15 frames per second) for each set of operating parameters. A custom code was developed using the OpenCV, computer vision Python library to classify the drop type as normal, nodrop, or satellite from the videos. The droplet velocity and volume values for each input parameter combination were calculated from the image analysis. The input and output parameters were saved as a .csv file, which served as the dataset. Python programming language was used in Jupyter notebook for data pre-processing, feature selection, spot check classification and regression algorithms, model selection, and to plot the needed visuals. Fujifilm's Model 3 fluid was used to print a selected pattern. A Samba cartridge with a drop volume of 2.4pL and a drop size of 17 microns was used to conduct the experiments. The pattern used to run the experiments is shown in Fig. 3. It was the same for all the runs.

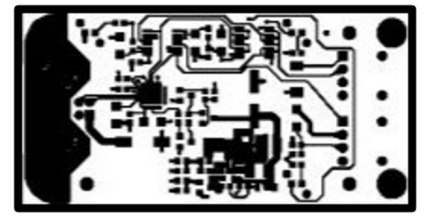


Fig. 3. Pattern (input drawing). [39]

The trajectory of the droplet is described as a drop ejecting from the nozzle vertically down onto either the drop catcher or substrate. This can be seen in Fig. 4a where the droplet ejects from the nozzle of the cartridge. The image captured will have a mirror image at the top. The camera captures the nozzle tip and the drop propagation from the nozzle to the drop catcher, as shown in Fig. 4b. whereby, image analysis was conducted to classify the drop characteristics and calculate the drop velocities and volumes.

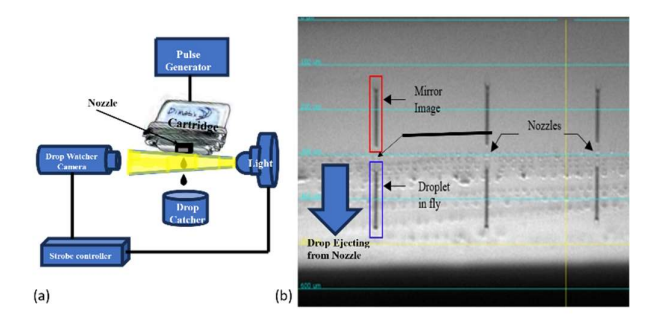


Fig. 4. Droplets eject from nozzle (a) physical set-up (b) drop travel image.

Initial experiments were conducted wherein changes were made to one independent variable at a time to avoid the influence of confounding variables. Thereby, we evaluate the extreme limits of the input parameters to eject droplets. Table. 1 shows the results for the limiting conditions. All experiments were carried out in a controlled environment at a temperature of 25 °C and a relative humidity of 60%.

Table. 1. Process parameter levels and output metrics.

Condition		No- Drop	Satellite	Normal
I. Voltage range	below 17V	X		
F=5, t=40, MV=3.5	18 to 27V			x
	28-30V		x	
II. Frequency range	1.18 to 7kHz			x
V=23, t=40, MV=3.5	8-13kHz			X
	13.1 and above		X	
III. Ink temp range	32°C	x		
V=23, F=5, MV=3.5	34-40			x
	42-46		x	
IV. Meniscus Vacuum range	3.5			x
V=23, F=5, t=40	4 and above		X	

Table. 2 shows the design matrix of some of the runs used for this experiment. It shows combinational values for all input parameters.

Table. 2. Sample data points of the design matrix.

Run Number (randomly	Voltage (V)	Frequency (kHz)	Ink Temperature	Meniscus Vacuum	
selected)			(°C)	(inches of H ₂ O)	
19	17	5	32	3.5	
59	32	10	38	4.5	
126	25	15	44	5.5	
343	21	8	28	4.0	

356	29	13	36	5.0
477	35	18	40	6.0

3.1.1. Velocity of droplet

Images captured from the drop watcher camera were used to find the droplet's velocity. Strobe delay was used in conjunction with the droplet distance from the nozzle in the captured frame. Strobe delay captured from the drop watcher video can be seen in Fig. 5, for a delay of 30 μ sec. The drop travelled 240 μ m and thus, the drop velocity was calculated as a ratio of the distance travelled and the strobe delay. In this illustration, the drop velocity was 8.0 m/s. In this work, python programming and image analysis through OpenCV are used to capture the velocities automatically and were exported into a .csv file.

The automated method is more precise and faster than the traditional method presented by [40], [41]. The images were captured for all the datasets, and the velocity for each dataset was fed into the machine learning algorithm for predictive analysis.



Fig. 5. Ink droplet travel for a strobe delay of 30 $\mu s.$

3.1.2. Droplet volume

Ink droplets were ejected in different forms based on the preset jetting conditions and the ink properties. To accommodate all forms of ink droplet shapes including spherical, elongated, and combinations thereof, the ink droplet volume was computed using the centroid approach as compared to the volume formula for simple spherical shape. For the centroid approach, a cross-sectional area of the ink droplet as shown in Fig. 6 was calculated. One-half of the cross-sectional area when rotated about its centroid in the vertical axis gives the volume of the droplet. This was further divided into smaller elemental parts, each having an area, ΔA_k . The total half of the droplet cross-sectional was summed as given in equation 1:

$$A = \sum_{k=1}^{n} \Delta A_k \tag{1}$$

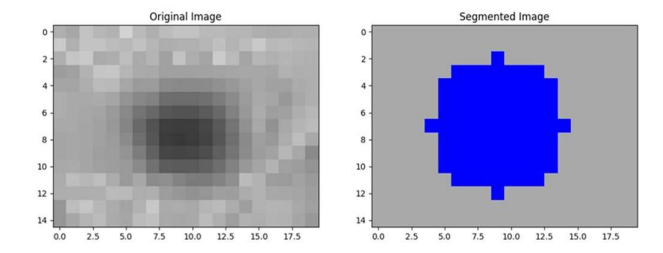


Fig. 6. Original and segmented ink droplet images for the region of interest.

The centroid of each elemental part is given as r_k . Using the concept of the moment of gyration, the centroid of half of the droplet cross-sectional area can be calculated using equation 2:

$$r_g = \frac{1}{4} \sum_{k=1}^n r_k \Delta A_k \tag{2}$$

The volume of the ink droplet was computed by rotating half of the droplet cross-sectional area by 2π and further simplification is given in equation 3:

$$Vol. = 2\pi \sum_{k=1}^{n} r_k \Delta A_k \tag{3}$$

Substituting equations 1 and 2 into equation 3, the general volume calculation using the centroid approach is given as:

$$Vol. = 2\pi r_q A \tag{4}$$

With equation 4, the droplet volume of any arbitrary shape can be computed such as non-spherical droplet shapes and elongated droplet shapes.

3.2. Data management

A crucial prerequisite before using datasets for any application is to understand the dataset at hand. Failure to do so can result in inaccurate analytics and unreliable decisions [42]. A total of 486 datasets were used in the prediction models.

3.2.1. Data collection and processing

The collection of data was based on experiments. Videos and images were captured through the DMP 2850 printer's drop watcher camera for each combination of input parameters as shown in Table 2. Strobe delay values for each dataset were captured to feed these values into the velocity calculations. The utmost care was taken to ensure consistency in the background of the videos and images to avoid region of interest conflicts while performing image extractions. The videos and images contain noise from various sources like misfiring at nozzles and clogging of ink or splashes. To avoid the confusion of classifying the droplet between normal and satellite, a customwritten Python code using OpenCV and NumPy libraries was used to perform background subtraction. The size of the original images were 720 pixels x 480 pixels x 3 channels for the width, height, and channels, respectively. The region of interest (a single nozzle and the ink droplet) was obtained by cropping the original image size to a width of 20 pixels and height of 240 pixels and retaining the 3 color channels that were

specified in the Python code used. The image reduction aided efficient computation for the measured ink droplet types, volume, and velocities.

The ANOVA (Analysis of Variance) shown in Table 3 represents the results of statistical analysis looking at the effects of individual factors of voltage, frequency, ink temperature, and meniscus vacuum on a droplet type (normal, satellite, or no droplet), as well as the interaction effects between these factors. Larger F-values (variances between two populations) typically signal a significant relationship between the factor and the droplet type. The p-value is the probability of observing a statistic as extreme as the one calculated under the null hypothesis (the hypothesis that there is no effect). Pvalue (probability of observing a statistic as extreme) less than 0.05 are usually taken as evidence that the factor significantly affects the outcome. In Table 3, the effects of voltage, ink temperature, and meniscus vacuum on the droplet type seem to be significant as the p-values are 0.0014, 0.0033, and 0.0065 respectively, which are less than 0.05. The interactions between voltage, frequency, ink temperature, and meniscus vacuum are not statistically significant, with p-values of 0.78 between voltage and frequency, 0.57 between voltage and ink temperature, 0.14 between voltage and meniscus vacuum, 1.00 between frequency and ink temperature, and 0.56 for frequency and meniscus vacuum. The factor frequency does not have a significant effect on its own with a p-value 0.64 (greater than 0.05).

Table 3. ANOVA table for main and interaction effects on droplet characteristics.

Source of variation	Sum of Squares	Degrees of Freedom	F-value	p-value
voltage	3.74	1	11.0	0.0014
frequency	0.074	1	0.218	0.64
ink temp	3.13	1	9.2	0.0033
Meniscus vac	2.67	1	7.85	0.0065
voltage: frequency	0.026	1	0.07	0.78
Voltage: ink temp	0.1	1	0.31	0.57
voltage: meniscus vac	0.75	1	2.2	0.1416
Frequency: ink temp	9.08E-28	1	2.67E-27	1
frequency: meniscus vac	0.11	1	0.33	0.56
Ink temp: meniscus vac	1.36	1	4.01	0.049

3.3. Machine learning algorithms

3.3.1. Classification algorithm for drop characteristics

Four machine learning models, random forest, support vector classifier, k-nearest neighbor, and decision trees, were used to classify droplet type as no-droplet, satellite, or normal. Model accuracy and confusion matrix were both used as classification metrics to determine each model's performance. K-fold cross-validation, which provides a more robust and comprehensive way to assess a model's performance and generalization was used compared to a simple train-test split. Hyperparameter tuning was also performed to explore the optimal hyperparameter selection for each model. Three k-fold values of 3, 5, and 8 were used on the 486 data points.

3.3.1.1. Classification performance metrics

The chosen classification models were evaluated using the model accuracy and confusion matrix as detailed in Section 4.

Model accuracy

Model accuracy is the ratio of rightly classified instances by the model to the total number of instances as expressed in equation 5. A higher model accuracy is desirable, and at the same time, the issue of overfitting was checked.

$$\frac{accuracy}{True\ Positive + True\ Negative} = \frac{True\ Positive + True\ Negative}{True\ Positive + False\ Positive} (5)$$

Confusion matrix

This is a table that shows the classification of data points into possible categories. The number of categories depends on the number of classes. In this work, three classes were considered, there are $3 \times 3 = 9$ possible categories.

3.3.2. Regression algorithms for drop velocity and volumes

Both ink droplet velocity and volume predictions were considered to be a regression problem because they are both continuous variables. Three linear models (linear, lasso, and ridge regression) and four non-linear models (random forest, decision tree, support vector regression, and k-nearest neighbor) were used to predict both the ink droplet volume and velocity. The mean squared error, the coefficient of determination, and the r-squared value were used to evaluate the performance of each model.

3.3.2.1. Regression performance metrics

The seven candidate regression models were evaluated using both the mean squared error, MSE, and the coefficient of determination, R^2 .

Mean squared error (MSE)

This is one of the most commonly used metrics to measure the performance of a regression predictive model. It measures the average squared difference between the actual and the model predicted values. Equation 6 shows how the mean squared error is calculated. A lower MSE value is mostly desirable as it depicts the regression model closely predicting the actual values.

$$MSE = \frac{1}{n} \sum_{i=1}^{n} (y_i - \hat{y}_i)^2$$
 (6)

where.

n is the total number of data points,

 y_i is the actual (experimental) value of the dependent for the ith data point,

 \hat{y}_i is the predicted value of the dependent for the i^{th} data point.

Coefficient of determination, R²

It measures the goodness of fit of a regression model. It quantifies the proportion of the variance in the dependent variable that can be predicted from the independent variable(s). Equation 7 shows how the coefficient of determination is measured.

$$R^2 = 1 - \frac{SSR}{SST} \tag{7}$$

where:

SSR - sum of squares of residuals, the sum of squared differences between the observed y values and the predicted y values from the regression model.

SST - total sum of squares, the sum of squared differences between each y value and the mean of all y values.

 R^2 value ranges from 0 to 1. A higher value closer to 1 is desirable as it shows that the regression model explains a larger portion of the variance in the dependent variable and the model fits the inkjet droplet data appropriately.

Model overfitting was checked with a new set of validation data as detailed in Subsection 4.4 of this work.

4. Results

In this section, first, the droplet type prediction is discussed based on the four classifiers. Both velocity and volume results are discussed in the next section for the seven regressors, and at k-fold values of 3, 5, and 8. All the classifiers and regressors are discussed at k-fold values of 3, 5, and 8, respectively.

4.1. Droplet type prediction

Both model accuracy and the confusion matrix were used to measure the performance of the classifiers at different values of k. The coded values for the droplet types include: (0 - no drop, 1 - satellite drop, 2 - normal drop). The confusion matrices shown in subsequent figures represent these coded values of the droplet type.

The mean of the accuracies obtained during k-iterations served as the model accuracy of the classifier at that given k-fold value. For constructing the model confusion matrix, all the k confusion matrices were aggregated. Then, for a normalized confusion matrix, each category on a row was divided by the row sum. Confusion matrices and accuracy plots are described in the following sections for the best model performers.

4.1.1. Model performance for droplet type prediction at k = 5

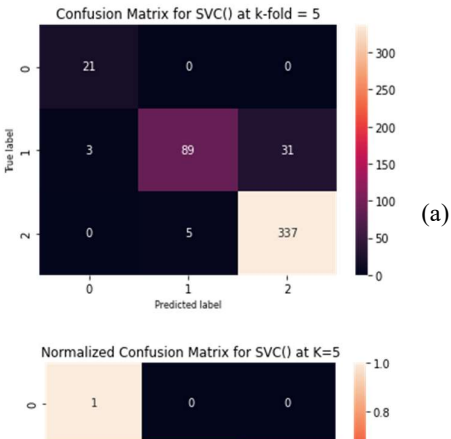
4.1.1.1. Confusion matrix at k = 5

All the classifiers at k = 5, perfectly classified the no-droplet type and there were improvements in the classification of normal droplets from the best at k = 3 which was 98% to 99% (see Fig. 7a and 7b, Fig 9a and 9b, Fig. 10a and 10b). The only exception in this case was for the random forest classifier at k = 3

= 5 which maintained its previous 98% as shown in Fig 8a and 8b

In the same trend at k=3, the support vector machine had the least classification for the satellite droplet with an accuracy of 72%, followed by the random forest classifier and k-nearest neighbor with accuracies of 85% and 89% respectively. Decision tree classifier was the highest with an accuracy of 91% for the satellite droplet type.

It is worthy of note that majority of the wrongly classified satellite data points were classified as normal and others as nodroplets.



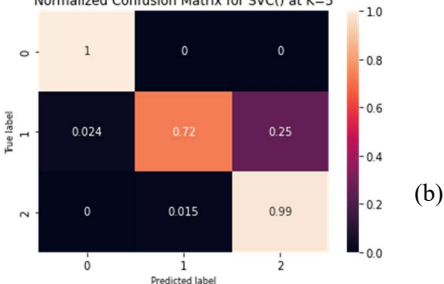
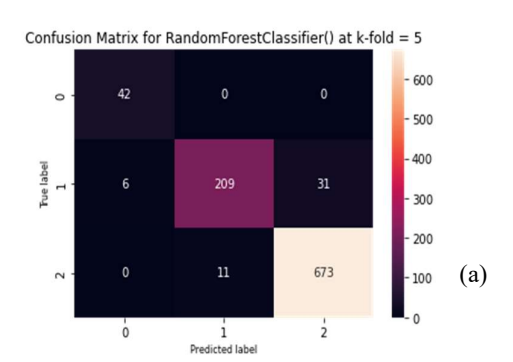


Fig. 7. Confusion matrices for droplet type prediction using support vector machine at k = 5, (a) aggregated and (b) normalized.



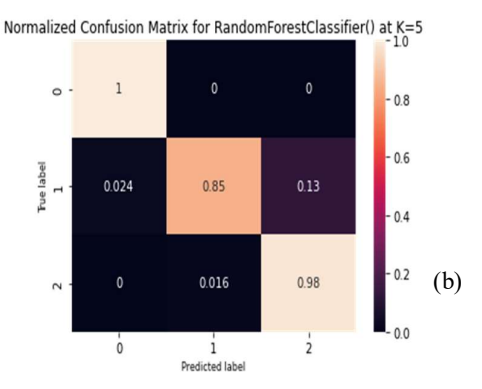
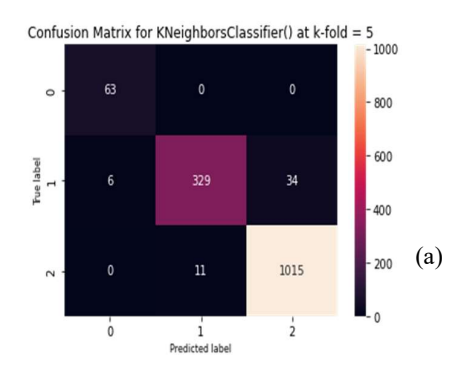


Fig. 8. Confusion matrices for droplet type prediction using random forest at k = 5, (a) aggregated and (b) normalized.



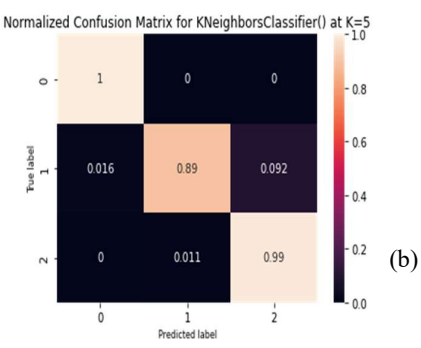
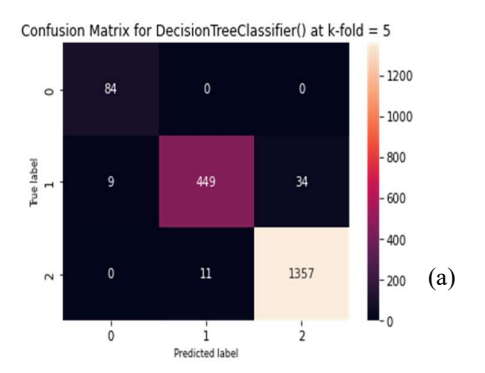


Fig. 9. Confusion matrices for droplet type prediction using k-nearest neighbor classifier at k = 5, (a) aggregated and (b) normalized.



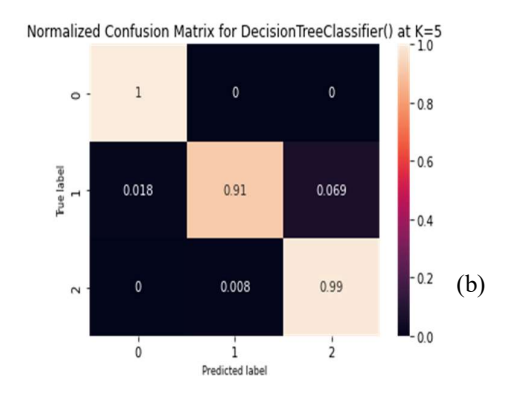


Fig. 10. Confusion matrices for droplet type prediction using decision tree at k = 5, (a) aggregated and (b) normalized.

4.1.1.2. Model mean accuracy at k = 5

The support vector machine has the least accuracy at 92% compared to other classifiers at k = 5. Relative to its previous value when k = 3, there is about 4% increase. In that order, random forest, k-nearest neighbor, and decision tree classifiers were all outstanding with mean accuracies of 98%, 99%, and 99%, as shown in Fig. 11.

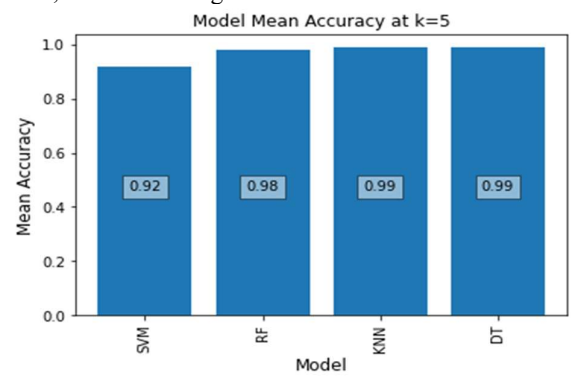


Fig 11. Mean model accuracies for all candidate classifiers at k=5.

In general, varying k from 3 to 5 showed great improvements for each droplet type classification. Also, the overall model mean accuracies improved- significantly as well. The results when k was increased from 5 to 8, despite the need for more computational works, showed minimal improvements and some led to the model behaving perfectly (a characteristic of overfitting).

4.2. Velocity prediction

Drop velocity was captured as the ratio of the maximum distance traveled from the nozzle to the strobe delay. To understand the relationship between the four input parameters and the droplet velocity, seven machine learning models were considered as regression predictors. Linear models (linear regression, lasso regression, and ridge regression) and nonlinear models (random forest, support vector regression, knearest neighbor regression, and decision tree) were the candidate models. The models were evaluated using both the mean squared error values and the R²-score to choose the best

model. A minimum mean squared value and a higher R²-score closer to 1 show a model that perfectly fits the inkjet droplet data set. Fig. 12 shows plot of the mean squared errors and the mean R²-scores for the candidate models at different k-fold values.

4.2.1. Best performance for velocity prediction at k = 5

The linear models have both their mean MSE and mean R^2 values to be the same as when k=3. The non-linear models shared the same trends for the mean MSE values except that the mean R^2 value increased from 0.97 to the decision tree regressor value of 0.98 and support vector regressor increased by 1% to 88% as shown in Fig. 12.

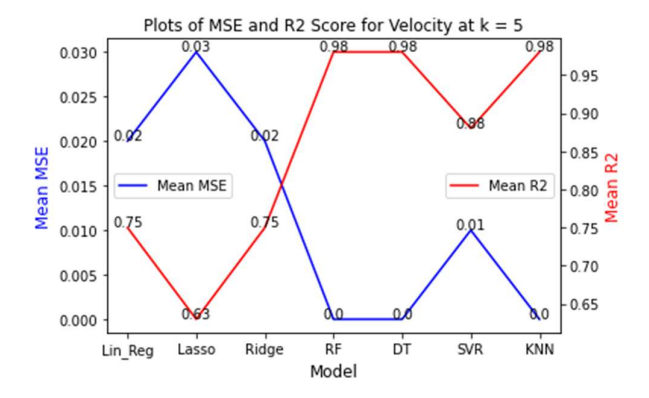


Fig. 12. Mean MSEs and mean R^2 -scores for all candidate models at k=5 for velocity prediction.

4.3. Volume prediction

Fig. 13, 14, and 15 show plots of the mean squared errors and the mean R²-scores for the candidate models at different k-fold values.

4.3.1. Model performance for volume predictions at k = 3, 5, and 8

The actual volume values were normalized for the entire dataset by dividing each value by the maximum volume since the difference between the actual and the predicted would be squared before obtaining the mean. The volume predictions at different k-fold values show similar trends to the velocity predictions but with slightly different values.

As the values of k increases, from k = 3 to 5, there were significant improvements for both mean MSE and mean R^2 values as seen in Fig. 13 and 14.

Increasing k from 5 to 8, tends to show minimal improvements of only about 1% across the mean MSE values as mean R^2 values stay the same as seen in Fig. 15.

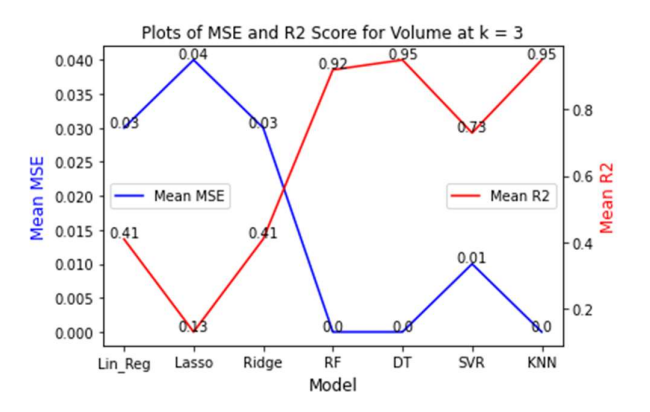


Fig 13. Mean MSEs and mean R^2 -scores for all candidate models at k = 3 for volume prediction.

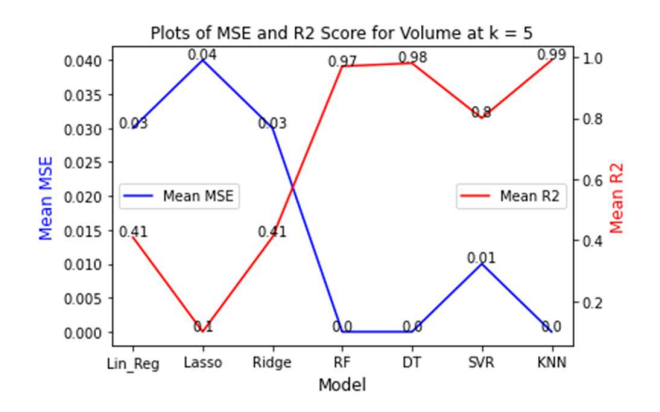


Fig. 14. Mean MSEs and mean R^2 -scores for all candidate models at k = 5 for volume prediction.

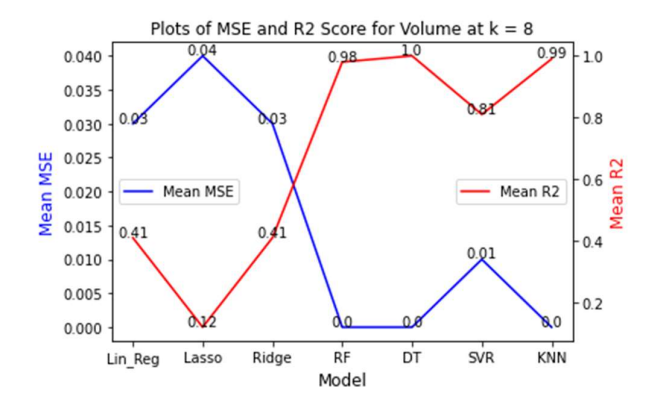


Fig. 15. Mean MSEs and mean R^2 -scores for all candidate models at k = 5 for volume prediction.

In general, at k = 5, either decision tree or k-nearest neighbor regressor predicts the velocity and volume with minimal mean MSE and mean R^2 values.

4.4. Experimental validation

Experimental validation was performed on a new set of 12 validation datasets to check and compare the best models for

drop type classifications, and regression prediction for drop velocity and drop volume at k-fold of 3, 5, and 8. The validation was carried out to check for overfitting, as that is how well each model generalizes. Across the three predicted outputs, k-fold value of 5, gave optimal model metrics without overfitting for the promising predictive models as summarized in Tables 4, 5, and 6 for the ink droplet type, velocity, and volume respectively.

4.4.1. Drop type validation

Table 4 shows the drop type predictions at the given input parameter values for the four considered classifiers against the experimental values. For each classifier, say at a given k-fold value, k number of predictions were made for each given set of input parameter values. Maximum voting, that is, the mode of the class, was chosen from the k number of predictions to represent the drop type class. A special case will be when k-fold value is 3 and for each iteration, the classifier classifies into distinct classes, say 0, 1, and 2. 0 which has no drop class is reserved for such scenarios. No such special case was encountered in this work. The validation results show that all the models irrespective of the chosen classifier and the k-fold value classified the drop type correctly. For reliability, k=5 was chosen as the best k-fold value for drop classification for any classifier as shown in Table 4.

4.4.2. Velocity validation

For the velocity, there was an improvement from k = 3 to k = 5. At k = 8, there was no or marginal improvement for the promising models. Thus, k = 5 was the overall best k-fold value, see Table 5. All the linear models failed to closely predict the velocity of the drop for the unseen data. Their velocity predictions were not surprising as they all have large MSE values of 0.02, 0.03, and 0.02 for linear regression, lasso, and ridge at k = 5 respectively as illustrated in Fig. 22 relative to the non-linear models. Also, their R^2 were very low, with the highest value of 0.41 for linear regression and ridge.

On the contrary, at k = 5, most of the non-linear models performed well across their MSE and R^2 values. All the models perfectly predicted the actual velocity with MSE values of 0 and R^2 values of 0.98 except the SVR which performed moderately well.

4.4.3. Volume validation

Table 6 shows the optimal value of k-fold of 5 for the considered regression models for the volume predictions. With similar trends for both MSE and R^2 values for the velocity predictions. All the linear models performed poorly with very low R^2 of 0.41 for linear regression and ridge with lasso having 0.1. Their poor performance is further buttressed by their higher MSE values relative to the non-linear models.

The non-linear models had higher R^2 values very close to 1 and their MSE values were perfect except for SVM which had an R^2 value of 0.88 and an MSE value of 0.1.

In summary, the developed models for predicting the inkjet droplet type, velocities, and volumes generalized the inkjet data without overfitting. Any of the candidate classifier at k=5, rightly classified the droplet type. For the velocities and volumes, the linear models underfit the given inkjet data irrespective of the chosen k-fold values. On the other hand, all

the non-linear models (random forest regressor, support vector regressor, decision tree regressor, and k-neighbor regressor) closely fit the data at k=5 except for the support vector regressor which gave relatively moderate results.

Table 4: Drop type predictions by candidate model classifiers and actual drop type on the validation set at the best k-fold value of 5.

	Input	Parameters			AI/ML Classifiers			Ground-truth values
v	f	t	mv	SVM3	RF3	KNN3	DT3	Experimental Drop Type
17	10	32	3.5	2	2	2	2	2
17	5	44	5.5	2	2	2	2	2
25	10	32	4.5	0	0	0	0	0
25	5	32	4.5	0	0	0	0	0
25	5	44	3.5	1	1	1	1	1
32	10	44	3.5	1	1	1	1	1
21	18	28	4.0	0	0	0	0	0
21	13	28	6.0	0	0	0	0	0
35	13	36	5.0	2	2	2	2	2
29	13	40	5.0	2	2	2	2	2
21	8	28	6.0	1	1	1	1	1
21	13	36	6.0	1	1	1	1	1

Table 5: Velocity predictions by candidate model regressors and actual velocity on the validation set at the best k-fold value of 5.

	Input F	Paramete	rs		AI/ML Regressors						Ground-truth values	
v	f	t	mv	Lin_Reg5	Lasso5	Ridge5	RF5	DT5	SVR5	KNN5	Experimental Velocity	
17	10	32	3.5	2.20	3.56	2.24	1.76	1.72	3.03	1.72	1.72	
17	5	44	5.5	3.57	3.72	3.59	3.37	3.37	3.29	3.37	3.37	
25	10	32	4.5	5.22	5.99	5.24	0.31	0.00	1.31	0.00	0.00	
25	5	32	4.5	5.47	5.99	5.48	0.15	0.00	1.32	0.00	0.00	
25	5	44	3.5	7.94	6.16	7.92	8.47	8.23	8.92	8.13	8.41	
32	10	44	3.5	11.16	8.59	11.11	9.24	9.07	9.48	9.07	9.07	
21	18	28	4.0	2.83	4.74	2.87	0.44	0.20	1.11	0.20	0.00	
21	13	28	6.0	2.18	4.74	2.23	0.36	0.24	1.43	0.24	0.00	
35	13	36	5.0	10.58	9.69	10.54	7.72	7.66	8.95	7.66	7.66	
29	13	40	5.0	8.12	+7.33	8.10	6.92	6.90	8.26	6.90	6.97	
21	8	28	6.0	2.43	4.74	2.47	1.51	1.54	2.80	1.54	1.54	
21	13	36	6.0	3.19	4.82	3.22	2.82	2.75	4.03	2.75	2.75	

Table 6: Volume predictions by candidate model regressors and actual volume on the validation set at the best k-fold value of 5.

Input Parameters						AI/ML Regressors				Ground-truth values		
v	f	t	mv	Lin_Reg5	Lasso5	Ridge5	RF5	DT5	SVR5	KNN5	Experimental Volume	
17	10	32	3.5	2462.63	3407.51	2478.96	2744.01	2873.36	4285.88	2873.36	2881.00	
17	5	44	5.5	3650.41	3682.71	3656.13	2356.38	2338.00	3399.48	2338.00	2333.00	
25	10	32	4.5	3234.05	3799.81	3241.37	197.52	0.00	897.16	0.00	0.00	
25	5	32	4.5	4195.58	3855.52	4194.33	414.10	0.00	1459.28	0.00	0.00	
25	5	44	3.5	7405.39	4235.99	7375.91	8081.18	8093.72	6967.48	7767.45	8295.00	
32	10	44	3.5	8209.81	4626.25	8171.15	11329.14	11498.96	10430.44	11498.96	11488.00	
21	18	28	4.0	852.23	3438.39	881.77	331.45	0.00	1002.89	0.00	0.00	
21	13	28	6.0	-175.28	3386.78	-136.84	101.93	28.48	1416.99	0.00	0.00	

35	13	36	5.0	5458.77	4495.77	5443.24	6884.40	7388.32	6884.81	7388.32	7386.00
29	13	40	5.0	4800.47	4213.21	4792.94	4097.42	4264.07	5685.21	4264.07	4265.00
21	8	28	6.0	786.24	3442.49	816.12	1069.23	1025.14	1579.65	1025.14	1022.00
21	13	36	6.0	932.36	3550.18	961.05	734.83	708.27	1918.37	661.15	658.00

All the datasets used to validate the drop characteristics were compared with actual images and the predictions had close agreement. Fig. 16 shows the actual images of all the datasets used for validation.

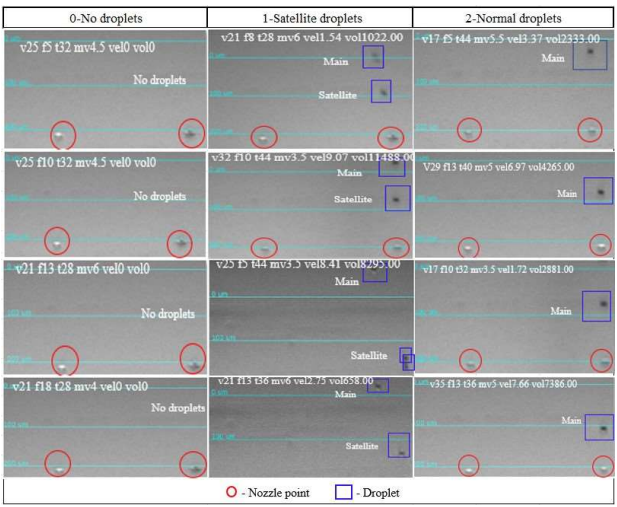


Fig. 16. Actual images and drop characteristics for the validation datasets.

5. Conclusions

3D materials inkjet printing has become a prominent additive manufacturing process with applications spanning the electronics, healthcare, and automotive domains. Although inkjet printing has been around for several decades, there is a lack of systematic know-how about the relationship between multiple input parameters and printing outcomes. Our group proposes an automated image analysis methodology that can capture droplet characteristics on-the-fly based on videos captured during printing. The custom OpenCV python image processing code developed in this research is utilized to identify different droplet conditions which include: no droplet, satellite droplet and normal droplet. The image processing algorithm was able to accurately identify these conditions by eliminating noise and extraneous features within the video frames. Moreover, droplet velocity and volume were calculated with high precision specifically for elongated and nonspherical droplets which frequently occur during the drop evolution phase after ejection from the nozzle. The ANOVA statistical measure revealed that voltage, ink temperature, and meniscus vacuum had a significant effect on the output metrics.

A multitiered machine learning strategy was implemented for predicting both qualitative droplet types and quantitative

droplet characteristics. In stage 1, classification algorithms including random forest (RF), support vector classifier (SVC), k-nearest neighbor (KNN), and decision trees (DT) models were utilized to predict droplet types. Among these, the RF,

KNN and DT models achieved the highest accuracy around 98% with a k = 5 folds design. Similarly, regression-based models for predicting droplet velocity and volume performed at optimal levels with k = 5 folds design based on hyperparameter optimization. This was also confirmed based on the confusion matrix results wherein, it is important to balance higher model accuracies with a substantial increase in computational times. This could be an important consideration when implementing these algorithms in real-time for process control, and higher latencies beyond a threshold may not be acceptable for practical applications. For the velocities and volumes, the linear models underfit the given inkjet data, irrespective of the chosen k-fold values. On the other hand, all the non-linear models (random forest regressor, support vector regressor, decision tree regressor, and k-neighbor regressor) closely fit the data at k = 5 except for the support vector regressor. Experimental validation of new test data sets showed close agreement between predicted outcomes of droplet type and actual velocities and volumes.

Future research would include correlating the in-flight droplet behavior with substrate deposition to obtain high fidelity printing, thus, providing a closed loop mechanism that can aid in the development of a digital twin model for a 3D material printer.

Acknowledgements

The authors would like to express their gratitude for funding support from the National Science Foundation Grant (NSF CMMI Awards #2100739, #2100850) and the Center of Excellence in Product Design and Advanced Manufacturing at North Carolina A&T State University.

References

- S. K. Parupelli and S. Desai, "A Comprehensive Review of Additive Manufacturing (3D Printing): Processes, Applications and Future Potential," Am. J. Appl. Sci., vol. 16, no. 8, pp. 244–272, 2019, doi: 10.3844/ajassp.2019.244.272.
- [2] B. P. Conner et al., "Making sense of 3-D printing: Creating a map of additive manufacturing products and services," Addit. Manuf., vol. 1, pp. 64–76, 2014, doi: 10.1016/j.addma.2014.08.005.
- [3] H. Elhoone, T. Zhang, M. Anwar, and S. Desai, "Cyber-based design for additive manufacturing using artificial neural networks for Industry 4.0," https://doi.org/10.1080/00207543.2019.1671627, vol. 58, no. 9, pp. 2841–2861, May 2019, doi: 10.1080/00207543.2019.1671627.
- [4] E. A. Guzzi, M. W. Tibbitt, E. A. Guzzi, and M. W. Tibbitt, "Additive manufacturing of precision biomaterials," Wiley Online Libr. Guzzi, MW TibbittAdvanced Mater. 2020•Wiley Online Libr., vol. 32, no. 13, Apr. 2019, doi: 10.1002/adma.201901994.
- [5] X. Zeng et al., "Additive manufacturing of precision optics at micro and nanoscale," Int. J. Extrem. Manuf., vol. 1, no. 1, p. 012005, Apr. 2019, doi: 10.1088/2631-7990/AB0FA5.
- [6] A. Awad et al., "A Review of State-of-the-Art on Enabling Additive Manufacturing Processes for Precision Medicine," J. Manuf. Sci. Eng., vol. 145, no. 1, Jan. 2023, doi: 10.1115/1.4056199/6941333/MANU-22-1279.PDF.

- [7] L. E. Murr and W. L. Johnson, "3D metal droplet printing development and advanced materials additive manufacturing," *Journal of Materials Research and Technology*, vol. 6, no. 1. pp. 77–89, 2017, doi: 10.1016/j.jmrt.2016.11.002.
- [8] L. Hirshfield, A. Giridhar, L. S. Taylor, M. T. Harris, and G. V Reklaitis, "Dropwise additive manufacturing of pharmaceutical products for melt-based dosage forms," *Elsevier*, vol. 103, no. 2, pp. 496–506, Feb. 2014, doi: 10.1002/jps.23803.
- [9] I. Gibson, D. Rosen, B. Stucker, and M. Khorasani, "Development of Additive Manufacturing Technology," *Addit. Manuf. Technol.*, pp. 23–51, 2021. doi: 10.1007/978-3-030-56127-7
- [10] N. Saengchairat, T. Tran, C. C.-V. and Physical, and undefined 2017, "A review: Additive manufacturing for active electronic components," *Taylor Fr. Saengchairat, T Tran, CK ChuaVirtual Phys. Prototyping*, 2017•Taylor Fr., vol. 12, no. 1, pp. 31–46, Jan. 2016, doi: 10.1080/17452759.2016.1253181.
- [11] C. Bailey, S. Stoyanov, T. Tilford, and G. Tourloukis, "Multi-physics models and condition-based monitoring for 3D-Printing of electronic packages," 2017, doi: 10.1109/EuroSimE.2017.7926286.
- [12] A. G. Frank, L. S. Dalenogare, and N. F. Ayala, "Industry 4.0 technologies: Implementation patterns in manufacturing companies," *Int. J. Prod. Econ.*, vol. 210, pp. 15–26, 2019, doi: 10.1016/j.ijpe.2019.01.004.
- [13] A. Paszkiewicz, M. Bolanowski, G. Budzik, Ł. Przeszłowski, and M. Oleksy, "Process of creating an integrated design and manufacturing environment as part of the structure of industry 4.0," *Processes*, vol. 8, no. 9, 2020, doi: 10.3390/PR8091019.
- [14] A. Haleem and M. Javaid, "Additive manufacturing applications in industry 4.0: A review," J. Ind. Integr. Manag., vol. 4, no. 4, Dec. 2019, doi: 10.1142/S2424862219300011.
- [15] M. Ogunsanya, J. Isichei, S. K. Parupelli, S. Desai, and Y. Cai, "In-situ droplet monitoring of inkjet 3D printing process using image analysis and machine learning models," in *Procedia Manufacturing*, 2021, vol. 53, pp. 427–434, doi: 10.1016/j.promfg.2021.06.045.
- [16] J. Cordeiro and S. Desai, "The effect of water droplet size, temperature, and impingement velocity on gold wettability at the nanoscale," *J. Micro Nano-Manufacturing*, vol. 5, no. 3, Sep. 2017, doi: 10.1115/1.4036891/369684.
- [17] Y. Guo, J. Peters, T. Oomen, and S. Mishra, "Control-oriented models for ink-jet 3D printing," *Mechatronics*, vol. 56, pp. 211–219, Dec. 2018, doi: 10.1016/j.mechatronics.2018.04.002.
- [18] N. Divakaran, J. P. Das, A. K. P V, S. Mohanty, A. Ramadoss, and S. K. Nayak, "Comprehensive review on various additive manufacturing techniques and its implementation in electronic devices," *Journal of Manufacturing Systems*, vol. 62. pp. 477–502, 2022, doi: 10.1016/j.jmsy.2022.01.002.
- [19] P. V. Raje and N. C. Murmu, "A Review on Electrohydrodynamic-inkjet Printing Technology," *Ijetae.Com*, vol. 4, no. 5, pp. 174–183, 2014, Accessed: Nov. 01, 2023. [Online]. Available: https://www.academia.edu/download/33817551/IJETAE_0514_29.pdf.
- [20] P. Smith, A. M.-J. of M. Chemistry, and undefined 2012, "Reactive inkjet printing," pubs.rsc.org, 2012, doi: 10.1039/C2JM30649B.
- [21] I. Rezanka, "Thermal inkjet: a review," Color Hard Copy Graph., p. 192, 1992, Accessed: Nov. 01, 2023. [Online]. Available: https://www.spiedigitallibrary.org/conference-proceedings-of-spie/1670/0000/Thermal-inkjet-a-review/10.1117/12.2322228.short.
- [22] H. Wijshoff, "Structure and fluid-dynamics in piezo inkjet printheads,"
- [23] K. Li, J. kao Liu, W. shan Chen, and L. Zhang, "Controllable printing droplets on demand by piezoelectric inkjet: applications and methods," *Microsyst. Technol.*, vol. 24, no. 2, pp. 879–889, Feb. 2018, doi: 10.1007/S00542-017-3661-9.
- [24] Ogunsanya, M., Isichei, J., & Desai, S. (2023). Grid search hyperparameter tuning in additive manufacturing processes. Manufacturing Letters, 35, 1031-1042.

- [25] Ogunsanya, M., & Desai, S. (2023). Physics-based and data-driven modeling for biomanufacturing 4.0. Manufacturing Letters, 36, 91-95.
- [26] S. H. Kang, S. Kim, D. K. Sohn, and H. S. Ko, "Analysis of drop-on-demand piezo inkjet performance," *Phys. Fluids*, vol. 32, no. 2, Feb. 2020, doi: 10.1063/1.5142023/13845503/022007_1_ONLINE.PDF.
- [27] S. Lim, P. D. Fleming, and M. Joyce, "A study of the jetting evolution of nanocopper ink and nanosilver ink with inkjet," *J. Imaging Sci. Technol.*, vol. 57, no. 2, 2013, doi: 10.2352/J.ImagingSci.Technol.2013.57.2.020506.
- [28] X. Han et al., "Droplet bouncing: Fundamentals, regulations, and applications," Wiley Online Libr. Han, J Li, X Tang, W Li, H Zhao, L Yang, L Wang Small, 2022 • Wiley Online Libr., vol. 18, no. 22, Jun. 2022, doi: 10.1002/smll.202200277.
- [29] T. Srivastava, S. Jena, S. K.- Langmuir, and undefined 2021, "Droplet impact and spreading on inclined surfaces," ACS Publ., vol. 17, no. 46, p. 45, Nov. 2021, doi: 10.1021/acs.langmuir.1c02457.
- [30] J. Du, Y. Zhang, and Q. Min, "Numerical investigations of the spreading and retraction dynamics of viscous droplets impact on solid surfaces," *Colloids Surfaces A Physicochem. Eng. Asp.*, vol. 609, 2021, doi: 10.1016/j.colsurfa.2020.125649.
- [31] J. Xiao et al., "Computational study of single droplet deposition on randomly rough surfaces: Surface morphological effect on droplet impact dynamics," ACS Publ., vol. 57, no. 22, pp. 7664–7675, Jun. 2018, doi: 10.1021/acs.iecr.8b00418.
- [32] J. Huang, L. J. Segura, T. Wang, G. Zhao, H. Sun, and C. Zhou, "Unsupervised learning for the droplet evolution prediction and process dynamics understanding in inkjet printing," *Addit. Manuf.*, vol. 35, p. 101197, Oct. 2020, doi: 10.1016/j.addma.2020.101197.
- [33] A. Caggiano, J. Zhang, V. Alfieri, F. Caiazzo, R. Gao, and R. Teti, "Machine learning-based image processing for on-line defect recognition in additive manufacturing," CIRP Ann., vol. 68, no. 1, pp. 451–454, 2019, doi: 10.1016/j.cirp.2019.03.021.
- [34] D. Wu and C. Xu, "Predictive modeling of droplet formation processes in inkjet-based bioprinting," *J. Manuf. Sci. Eng. Trans. ASME*, 2018, doi: 10.1115/1.4040619.
- [35] X. Lin, K. Zhu, J. Zhou, and J. Y. H. Fuh, "Intelligent modeling and monitoring of micro-droplet profiles in 3D printing," *ISA Trans.*, vol. 105, pp. 367–376, 2020, doi: 10.1016/j.isatra.2020.05.030.
- [36] T. Akter and S. Desai, "Developing a predictive model for nanoimprint lithography using artificial neural networks," *Mater. Des.*, vol. 160, pp. 836–848, 2018, doi: 10.1016/j.matdes.2018.10.005.
- [37] H. Almakaeel, A. Albalawi, and S. Desai, "Artificial neural network based framework for cyber nano manufacturing," *Manuf. Lett.*, vol. 15, pp. 151– 154, Jan. 2018, doi: 10.1016/J.MFGLET.2017.12.013.
- [38] M. Ogunsanya and S. Desai, "Predictive Modeling of Additive Manufacturing Process using Deep Learning Algorithm," in Proceedings of the IISE Annual Conference & Expo 2022, 2022.
- [39] I. FUJIFILM Dimatix, "Dimatix Materials Printer DMP-2800 Series User Manual," FUJIFILM Dimatix, pp. 1–93, 2006, Accessed: Nov. 01, 2023. [Online]. Available: https://www.lcinet.kent.edu/images/user_images/cpip/1418077287_1879 5DMP-2800 User Manual v1.3.pdf.
- [40] L. Jagannathan, Organic and Printed Electronics for Biological Microfluidic Applications. 2012.
- [41] A. Rida, L. Yang, and M. M. Tentzeris, "Design and characterization of novel paper-based inkjet-printed UHF antennas for RFID and sensing applications," in *IEEE Antennas and Propagation Society, AP-S International Symposium (Digest)*, 2007, pp. 2749–2752, doi: 10.1109/APS.2007.4396104.
- [42] A. Jain et al., "Overview and importance of data quality for machine learning tasks," dl.acm.orgA Jain, H Patel, L Nagalapatti, N Gupta, S Mehta, S Guttula, S Mujumdar, S AfzalProceedings 26th ACM SIGKDD Int. Conf. knowledge ..., 2020•dl.acm.org, pp. 3561–3562, Aug. 2020, doi: 10.1145/3394486.3406477.